Structural instability of metallic glasses under radio-frequency-ultrasonic perturbation and its correlation with glass-to-crystal transition of less-stable metallic glasses

AUTHOR(S):

Ichitsubo, T; Matsubara, E; Chen, HS; Saida, J; Yamamoto, T; Nishiyama, N

CITATION:

Ichitsubo, T ...[et al]. Structural instability of metallic glasses under radio-frequency-ultrasonic perturbation and its correlation with glass-to-crystal transition of less-stable metallic glasses. JOURNAL OF CHEMICAL PHYSICS 2006, 125(15): 154502.

ISSUE DATE:

2006-10-21

URL:

http://hdl.handle.net/2433/39774

THE JOURNAL OF CHEMICAL PHYSICS **125**, 154502 (2006)

Structural instability of metallic glasses under radio-frequency-ultrasonic perturbation and its correlation with glass-to-crystal transition of less-stable metallic glasses

T. Ichitsubo[a] and E. Matsubara
Department of Materials and Science Engineering, Kyoto University, Kyoto 606-8501, Japan

H. S. Chen[b]
Bell Laboratories, Lucent Technology, Murray Hill, New Jersey 07974

J. Saida
Center for Interdisciplinary Research, Tohoku University, Sendai 980-8578, Japan

T. Yamamoto
Institute for Materials Research, Tohoku University, Sendai 980-8577, Japan

N. Nishiyama
R & D Institute of Metals and Composites for Future Industries (RIMCOF), Sendai 980-8577, Japan

(Received 16 July 2006; accepted 18 July 2006; published online 16 October 2006)

It has been reported that the structural stability is significantly deteriorated under radio-frequency-ultrasonic perturbation at relatively low temperatures, e.g., near/below the glass transition temperature T_g, even for thermally stable metallic glasses. Here, we consider an underlying mechanism of the ultrasound-induced instability, i.e., crystallization, of a glass structure to grasp the nature of the glass-to-liquid transition of metallic glasses. Mechanical spectroscopy analysis indicates that the instability is caused by atomic motions resonant with the dynamic ultrasonic-strain field, i.e., atomic jumps associated with the β relaxation that is usually observed for low frequencies of the order of 1 Hz at temperatures far below T_g. Such atomic motions at temperatures lower than the so-called kinetic freezing temperature T_g originate from relatively weakly bonded (and/or low-density) regions in a nanoscale inhomogeneous microstructure of glass, which can be straightforwardly inferred from a partially crystallized microstructure obtained by annealing of a Pd-based metallic glass just below T_g under ultrasonic perturbation. According to this nanoscale inhomogeneity concept, we can reasonably understand an intriguing characteristic feature of less-stable metallic glasses (fabricated only by rapid melt quenching) that the crystallization precedes the glass transition upon standard heating but the glass transition is observable at extremely high rates. Namely, in such less-stable metallic glasses, atomic motions are considerably active at some local regions even below the kinetic freezing temperature. Thus, the glass-to-crystal transition of less-stable metallic glasses is, in part, explained with the present nanoscale inhomogeneity concept. © *2006 American Institute of Physics*. [DOI: 10.1063/1.2346672]

I. INTRODUCTION

In many alloy systems, amorphous state can be obtained by rapid melt quenching, but in some alloys it can be obtained even at a much slower quenching rate, e.g., of the order of 1–100 °C/s.[1–5] These amorphous alloys usually exhibit the glass-to-liquid transition upon heating and, therefore, called "metallic glasses."[6] Especially, the so-called bulk metallic glasses (BMGs) have excellent thermal stability against crystallization, despite the fact that they are composed mainly of metallic bonds unlike major glasses having network structures consisting of covalently bonded networks or clusters, such as SiO_2 and GeO_2. Hence, investigation of the origin of their excellent thermal stability (how can metallic glasses be formed stably?) has been one of fascinating issues in the BMG science.[7]

In general, around or below the glass transition temperature T_g, kinetic processes are substantially frozen, so that the system becomes nonergodic. Therefore, in most of the glasses, the glass transition is observed prior to crystallization upon heating (i.e., $T_g < T_x$), because the constituent molecules/atoms hardly move in the frozen amorphous state below T_g, where T_x means the crystallization onset temperature. Similarly, in stable metallic glasses, the distinct glass transition is observed prior to crystallization like other types of glasses, but in less-stable metallic glasses (so-called amorphous alloys) crystallization precedes the glass transition, i.e., $T_x < T_g$. The glass transition is, however, observable at extremely high heating rates,[8–10] because T_g is not sensitive to the heating rate, whereas T_x considerably increases with increasing heating rate. Namely, the controversial temperature relation $T_x < T_g$ indicates that constituent atoms are appreciably mobile even below such a kinetic freezing temperature T_g. This feature sounds quite eccentric and is

[a]Electronic mail: tichi@mtl.kyoto-u.ac.jp
[b]Retired.

exceptional for metallic glasses and rarely observed for other kinds of glasses. From this viewpoint, it is intriguing to consider the reversible glass-liquid transition and crystallization of metallic glasses.

Recently, in the process of determining the elastic moduli of some BMGs around the glass transition temperature, we have found that crystallization is much accelerated around the glass transition temperature T_g under ultrasonic (US) perturbation.[11–14] Similar phenomena were reported. Kopcewicz *et al.* showed lots of works on the effects of radio-frequency (rf) magnetic field on crystallization of some ferrous amorphous alloys.[15–17] They discussed that rf magnetostrictive vibration is responsible for the acceleration of crystallization. Similarly, Gupta *et al.* also reported that ultrasonic vibrations enhance the crystallization process of an Fe–Si–B–C amorphous alloy.[18] In a more recent work, significant reduction of T_g and T_x was also found during the ultrasonic pulse-echo measurements for a $Zr_{55}Al_{10}Ni_5Cu_{30}$ metallic glass.[19] As for the other anomalies, for example, Mizubayashi *et al.*[20] and Mizubayashi and Okuda[21] studied the effects of pulsed electric currents on the structural relaxation and crystallization of some kinds of amorphous alloys and showed that crystallization is accelerated at a temperature far below the normal crystallization temperature T_x. Independently, Teng *et al.*[22] and Lai *et al.*[23] also reported the similar electropulsing effects.

These phenomena indicate that the structural stability of metallic glasses is deteriorated under dynamic external fields even at relatively low temperature (below T_g). As described in the literature,[24] only the β (secondary) relaxation process remains active in the temperature range ($T<T_g$) where the system is completely frozen with respect to the α (primary) relaxation process (dynamic glass transition). It is, therefore, considered that the β relaxation[25–32] is responsible for the low-temperature instability under ultrasonic perturbation. In this paper, on the basis of our previous results for $Zr_{55}Al_{10}Ni_5Cu_{30}$ (Ref. 11) and $Pd_{40}Ni_{40}P_{20}$ (Refs. 12 and 13) and recent new results obtained for $Pd_{42.5}Ni_{7.5}Cu_{30}P_{20}$, we consider the underlying mechanism from the viewpoints of the β relaxation and the microstructural insight. The above-mentioned controversial temperature relation, $T_x<T_g$, for less-stable metallic glasses can be understood with the inhomogeneous structural model for fragile metallic glasses, which was inferred from a partially crystallized microstructure obtained by the ultrasonic annealing in the vicinity of T_g.[33]

II. CRYSTALLIZATION UNDER ULTRASONIC PERTURBATION

A. Experimental procedure

Alloy ingots of $Zr_{55}Al_{10}Ni_5Cu_{30}$, $Pd_{40}Ni_{40}P_{20}$, and $Pd_{42.5}Ni_{7.5}Cu_{30}P_{20}$ (at. %) BMGs were used in this work. The glass transition temperatures T_g of each specimen were determined using the differential scanning calorimeter (DSC) (Perkin Elmer). At heating rates lower than 20 °C/min, T_g of each sample is about 390–400 °C for $Zr_{55}Al_{10}Ni_5Cu_{30}$ and 290–300 °C for $Pd_{40}Ni_{40}P_{20}$ and $Pd_{42.5}Ni_{7.5}Cu_{30}P_{20}$.

To carry out annealing at elevated temperatures under US vibrations (US annealing), we employed the electromagnetic acoustic resonance (EMAR) method (RAM-10000, RITEC Inc), in which acoustic vibrations are generated by the Lorentz force mechanism.[11–13] Samples of cylindrical shape of about $\phi 3\times 4$ mm^2 were inserted into the electromagnetic acoustic transducer (EMAT). Resonance frequencies f_r of the cylindrical samples were detected in a radio-frequency (sub-/low-megahertz frequency) range. Internal friction (ultrasonic attenuation coefficient) was measured at each resonance frequency by the free-decay method,

$$A(t) = A_0 \exp(-Q^{-1}\pi f_r t), \tag{1}$$

where A and f_r denote the amplitude and the resonance frequency, respectively, and Q^{-1} represents the internal friction.

In our ultrasonic measurements, heating effect due to eddy currents must be taken into consideration. Then, the sample surface temperature was monitored using a fully crystallized dummy sample with a Pt–PtRh thermocouple and the heating effect due to the eddy currents was taken into account; all graphs are displayed using the sample surface temperature. The ultrasonic measurements were performed under a pressure of about 10^{-3} Pa at elevated temperatures.

B. Ultrasonic effects on crystallization above T_g

Figure 1(a) shows the time-temperature -transformation (TTT) diagram obtained for a $Pd_{42.5}Ni_{7.5}Cu_{30}P_{20}$ glass with or without US perturbation. The time in the lateral axis denotes the duration required for completing the crystallization (hereafter, referred to as "crystallization time"). The crystallization time was easily judged from the significant change in the resonance frequencies in the case of the US annealing. As for the normal annealing without US, it was estimated from disappearance of the exothermic heat in DSC. The US-annealing treatments were performed slightly above T_g. Under US perturbation, the crystallization is very much accelerated. As shown elsewhere,[14] we have also investigated the crystalline phases formed under US perturbation and concluded that the US annealing merely enhances the crystallization rate but produces no particular phases.

The strain-amplitude dependence of the crystallization time was also investigated at 330 °C ($>T_g$) by changing the peak-to-peak voltage applied to an EMAT coil. The result is shown in Fig. 1(b). The absolute magnitude of the US strain was not determined in this study, but it increases with increase in the EMAT voltage. Apparently, the crystallization time becomes shorter when the strain amplitude of US vibrations is larger.

C. Internal friction in radio-frequency range and its correlation with the β relaxation

At the dynamic glass transition, the typical relaxation time usually becomes of the order of 1–100 s, so that the characteristic frequency should become reciprocal values. Therefore, low-frequency internal-friction measurements have been frequently performed so far; it is known that Q^{-1} is inversely proportional to a measurement frequency f.[34,35] However, we can detect Q^{-1} at megahertz frequencies around T_g for $Zr_{55}Al_{10}Ni_5Cu_{30}$ and $Pd_{40}Ni_{40}P_{20}$ BMGs by the

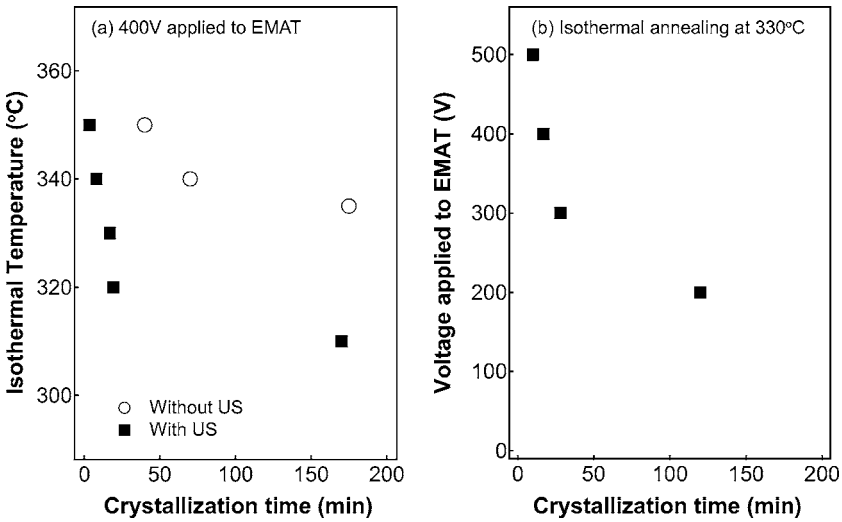

FIG. 1. (a) Time-temperature-transformation diagram for $Pd_{42.5}Ni_{7.5}Cu_{30}P_{20}$ with or without ultrasonic perturbation (with US/without US). The time in the lateral axis indicates the duration required for completing crystallization. Peak-to-peak voltage applied to the EMAT coil was 400 V and ac frequency was about 1.2 MHz. The sample surface temperature is used for depicting the TTT diagram. (b) The amplitude dependence of the crystallization time at 330 °C for $Pd_{42.5}Ni_{7.5}Cu_{30}P_{20}$. The vertical axis shows the peak-to-peak voltage applied to an EMAT coil, and the strain amplitude is larger as the voltage is higher.

EMAR method; $Q^{-1}(T)$ and $f_r(T)$ curves are shown in Fig. 2(a). It is obviously found that $Q^{-1}(T)$ increases steeply around T_g and is sharply diminished about T_g. Simultaneously $f_r(T)$ decreases and jumps up. The drastic change in $f_r(T)$ is attributed to the US-accelerated crystallization.

We next consider what causes such an increase of Q^{-1} at megahertz frequencies. According to the diffusion data,[36,37] the activation energy ΔE_{diff} of diffusion of Ni in $Pd_{40}Ni_{40}P_{20}$ is about 3 eV, and that in $Zr_{55}Al_{10}Ni_5Cu_{30}$ is about 1 eV. Since the Debye frequency ν_D is of the order of 10^{13} Hz, the successful jump frequency around T_g is $\nu(T_g) = \nu_D \exp(-\Delta E_{\mathrm{diff}}/kT_g) \sim 10^{-13}$ Hz for $Pd_{40}Ni_{40}P_{20}$ and $\nu(T_g) \sim 10^5$ Hz for $Zr_{55}Al_{10}Ni_5Cu_{30}$, where k is the Boltzmann constant. The latter frequency is close to the US frequencies used in this study, but the former is much smaller than the US frequencies. Therefore, we should consider some atomic motions different from the long-range diffusion.

Here we take notice of the β relaxation. The activation energy for the β relaxation is known to be far lower than that for the α relaxation in which cooperative atomic motions occur with a high activation energy.[26] Actually, the β relaxation was observed, for example, in Pd–Cu–Si,[27] La–Al–Ni,[28,29] and Pd–Ni–Cu–P glasses.[30] While the α relaxation is observed around T_g at a low frequency (~1 Hz), the β relaxation is observed far below T_g at the same frequency.[26] In order to evaluate a temperature range of the β relaxation in the present frequencies, the $Q_\beta^{-1}(T)$ curves are calculated for a megahertz frequency range by using $\Delta E_\beta \sim 1.0$ eV and $\tau_0 \sim 1.0 \times 10^{-14}$ s (which were obtained with low-frequency internal-friction measurement for a Pd–Ni–Cu–P glass by Pelletier *et al.*[30]) with the Debye function

$$Q_\beta^{-1} = \Delta_Q \frac{\omega\tau}{1+(\omega\tau)^2}, \tag{2}$$

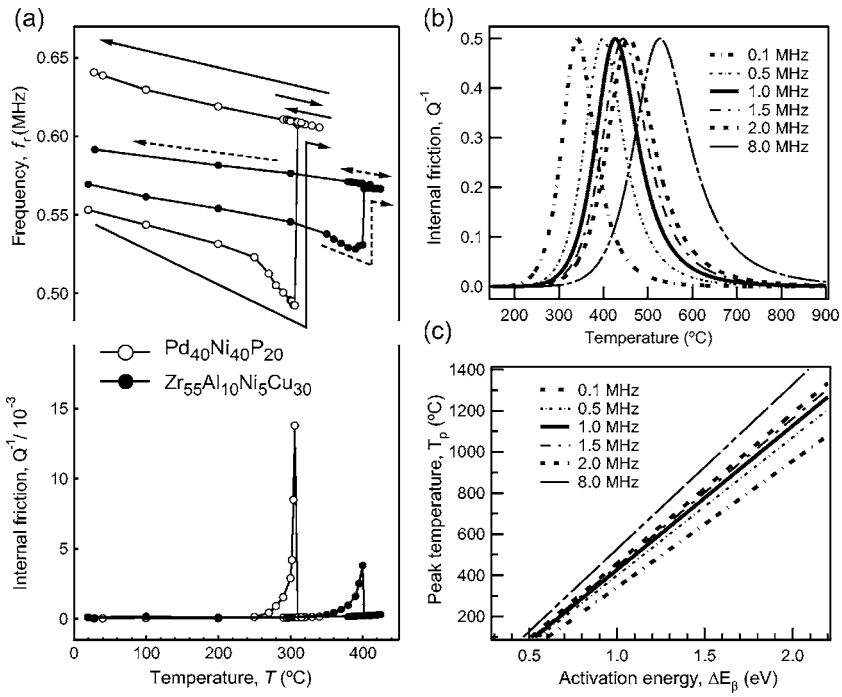

FIG. 2. (a) Radio-frequency internal friction and resonance frequency as a function of temperature, obtained for fully structurally relaxed samples of Pd- and Zr-based metallic glasses. (b) Temperature dependence of the internal friction calculated for the β relaxation in a Pd-based metallic glass. $Q^{-1}-T$ curves calculated using Eqs. (2) and (3) with $\Delta E_\beta \sim 1.0$ eV and $\tau_0 \sim 1.0 \times 10^{-14}$ s. (c) The activation-energy (ΔE_β) dependence of the peak temperature (T_p) that satisfies $\omega\tau = 1$.

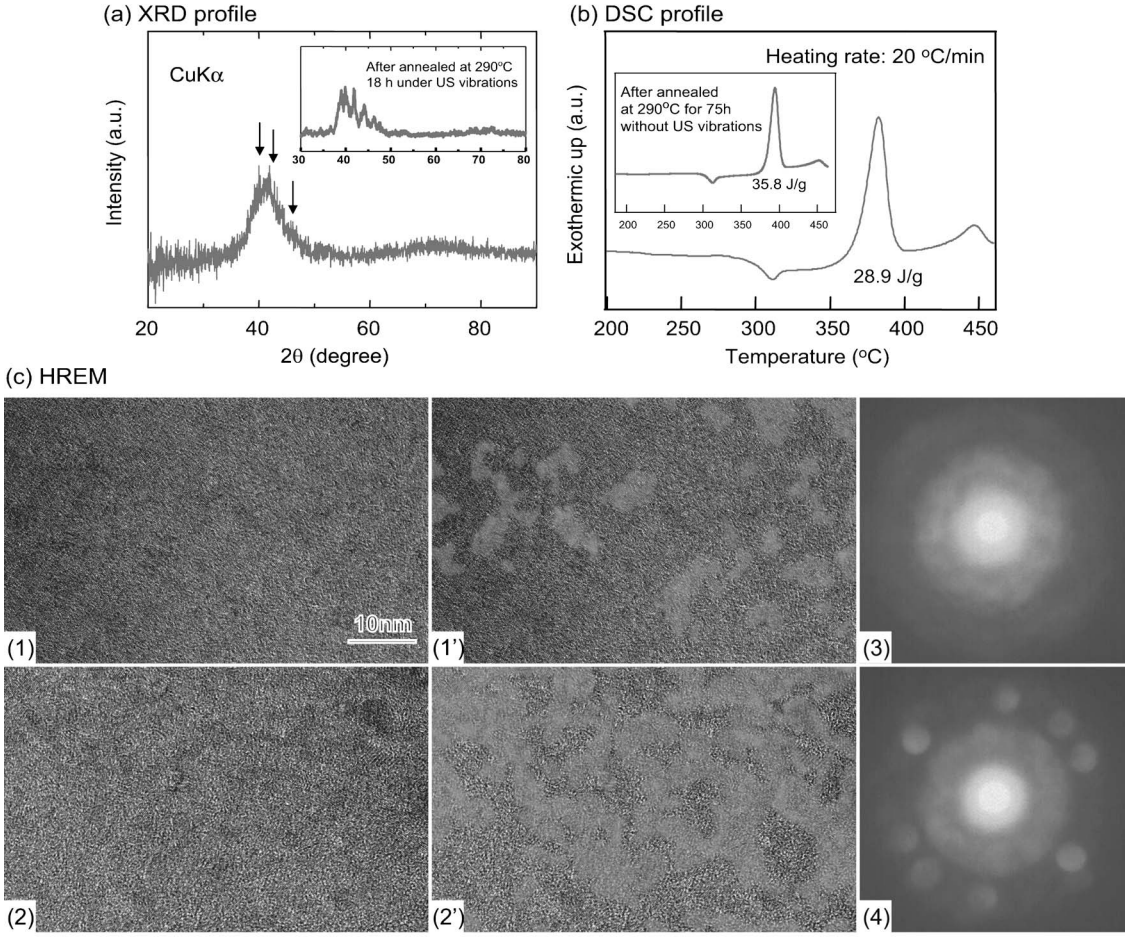

FIG. 3. $Pd_{42.5}Ni_{7.5}Cu_{30}P_{20}$ metallic glass after being annealed at 290 °C (below T_g) for 10 h under US vibrations of 0.35 MHz. (a) X-ray diffraction profiles, (b) DSC profile, and (c) HREM images [(1) and (2′)] and nanobeam diffraction (NBD) patterns [(3) and (4)]. For comparison, the inset of (a) shows the x-ray diffraction profile after annealed at 290 °C for 18 h under US vibrations and the inset of (b) shows the DSC trace after being annealed at 290 °C for 75 h without US vibrations. In (c), the HREM sample was prepared by ion milling with cooling using liquid N_2 to prevent crystallization due to ion irradiation. Figures (1) and (2) are original images, and in (1′) and (2′) crystallized regions are colored for the sake of conspicuity. The NBD pattern (3) was taken in the relatively less crystallized regions, and NBD (4) was taken in the more crystallized regions.

$$\tau = \tau_0 \exp\left(\frac{\Delta E_\beta}{kT}\right), \tag{3}$$

where Δ_Q is the relaxation strength, $\omega(=2\pi f)$ is the angular frequency (f is the frequency of oscillator), τ is the relaxation time per event, τ_0 being the atomic-molecular-scale time, and ΔE_β is the activation energy of the event. Figure 2(b) shows the calculated internal friction $Q_\beta^{-1}(T)$ for the β relaxation and clearly indicates that the experimental $Q^{-1}(T)$ curves at the megahertz frequencies around T_g in Fig. 2(a) correspond to the rising edges of the calculated profile of Fig. 2(b). In addition, since the relation $\omega\tau=1$ holds at the peak temperature T_p in Eq. (2), T_p is given by

$$T_p = -\frac{\Delta E_\beta}{k \ln \omega\tau_0}. \tag{4}$$

The peak temperature T_p is shown in Fig. 2(c) as a function of the activation energy ΔE_β. T_p is very sensitive to ΔE_β, and the increase of the internal friction occurring around 300–400 °C can be explained well with the ΔE_β value for the β relaxation (~1 eV).

Thus, in the case of Pd-based metallic glasses, the β relaxation observed far below T_g at low frequencies is detected at a temperature around or higher than T_g at megahertz frequencies. On the assumption that the activation energy of the β relaxation in $Zr_{55}Al_{10}Ni_5Cu_{30}$ is close to 1 eV, the same discussion is applicable.

D. Partially crystallized microstructural pattern obtained by US-annealing near/below T_g

If the US-accelerated crystallization is related to the β relaxation, this must take place even below T_g. We have verified this for $Pd_{42.5}Ni_{7.5}Cu_{30}P_{20}$ by performing the isothermal annealing at 290 °C for 18 h under radio-frequency vibrations of about 0.35 MHz. The x-ray diffraction profile in the inset of Fig. 3(a) indicates that the US-annealed sample was sufficiently crystallized. In the case of annealing without ultrasonic vibrations for 75 h at this temperature, no crystallization was observed; see the inset of Fig. 3(b).

Next, we annealed a sample at 290 °C for 10 h with US vibrations to obtain a mixture consisting of mainly amorphous regions with a small amount of crystallized regions. Figure 3 shows (a) x-ray diffraction profiles, (b) DSC, and

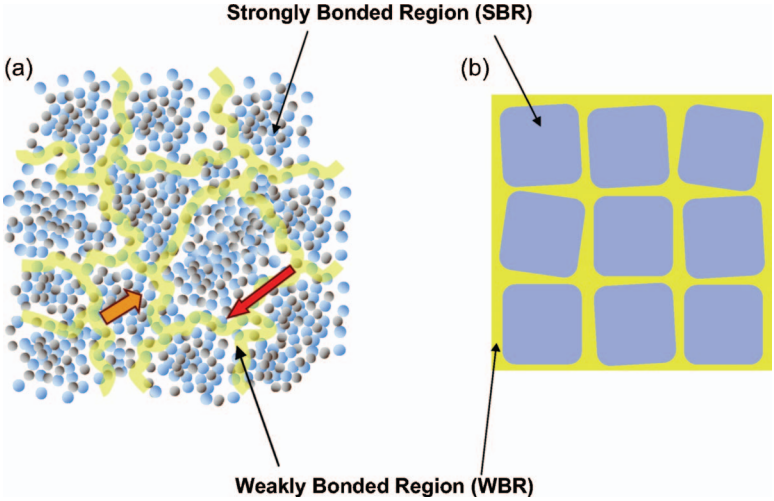

FIG. 4. (Color) (a) Microstructural model of fragile metallic glasses inferred on the basis of the microstructure of the US-annealed sample, Fig. 3(c). (b) Simplified model. In this model, the glassy substances are comprised of two parts: strongly bonded regions (SBRs) and weakly bonded regions (WBRs) (Ref. 33). The atomic mobility in WBRs is higher than that in SBRs.

(c) the high-resolution electron microscopy (HREM) images and nanobeam diffraction (NBD) patterns for the sample. Small diffraction peaks due to the crystalline phases are seen with a halo pattern of the amorphous phase in Fig. 3(a). The remaining amorphous fraction was roughly estimated to be about 80% from Fig. 3(b), since the crystallization heat around T_x is about 36–37 J/g. These results show that the sample was of mostly amorphous state containing a small amount of crystalline phases.

In Fig. 3(c), it is found that the US-induced microstructure is not so uniform; there exist regions where crystallization considerably proceeds [see (2), (2′) or (4)] and does not so proceed [see (1), (1′), or (3)]. We can see a very intriguing microstructure that the amorphous regions are surrounded by crystallized walls. This microstructure of the partially crystallized sample is obviously distinguished from a typical microstructure without US perturbation at a very early stage of crystallization,[38] in which submicron isolated crystals are formed in the amorphous matrix. In addition, since the growth of crystallized regions is quite slow in the case of the US-accelerated crystallization at such a low temperature, temperature increase by the exothermic heat due to crystallization is small and very fine nanocrystals (about 5 nm) are formed. This is considerably different from the microstructure obtained by the US annealing above T_g.[14]

III. MECHANISM OF STRUCTURAL INSTABILITY UNDER ULTRASONIC PERTURBATION

A. Stochastic resonance of atomic motions with ultrasonic strain

In vibration motions, the elastic strain energy and kinetic energy are converted to each other from moment to moment; here, we consider the maximum strain energy as a representative of the ultrasound energy. Since the elastic strain ϵ of US vibration is of the order $\epsilon \sim 10^{-5}$ (or 10^{-6}), the strain energy by US vibrations is estimated to be at most, $(\Omega/2)M\epsilon^2 \sim 10^{-28}$ J/at., where $\Omega(\sim 10^{-29}$ m^3/at.) is the atomic volume and $M(\sim 100$ GPa) is the elastic modulus. In contrast, thermal energy per atom, kT, around $T_g(500-700$ K) approximates about $\sim 10^{-20}$ J/at. (of the order of 10–100 meV). Hence, the US strain energy is found to be infinitesimally small compared with the thermal energy and the US-induced instability cannot be understood by the assistance to thermal agitation of atoms. However, if the stress of US vibrations interacts with defects such as vacant sites, the interaction energy is $\Omega M\epsilon \sim 10^{-23}$ J/at. As observed in Snoek relaxation, the order of this energy would be enough to modify the potential energy, especially for the glassy alloys in which the interatomic potential minima are not fixed as in crystal lattices.

Also from the above viewpoint, the β relaxation is the most possible candidate for explaining the US-induced instability. Actually, the increase of internal friction in Fig. 2(a) means that a periodic external strain is stochastically resonant with certain atomic motions and, from Figs. 2(b) and 2(c), it is reasonable to consider that these motions are associated with the β relaxation. In the absence of US strains atomic jumps occur repeatedly at the same sites, but in contrast, atomic jumps will become different from the ordinary ones under resonant periodic stress/strain fields, that is, atoms will move into more stable potential (energetically preferential) sites newly caused due to the strain. This situation resembles the Snoek relaxation. However, since the amorphous structure is not in thermodynamical equilibrium, repetition of such jumps will gradually change the energy landscape, eventually leading to crystallization.

B. Microstructural model

As was demonstrated in Fig. 3(c), we can crystallize the sample under US perturbation near/below T_g. It is reasonable to consider that the structural instability at such a low temperature is related to the β relaxation. Therefore, taking notice of the crystallized regions, we can prefigure the intrinsically mobile/soft regions in the amorphous matrix. From this viewpoint, we have recently proposed a plausible microstructural model shown in Fig. 4, in which the glassy solid is composed of strongly bonded regions (SBRs) and weakly bonded regions (WBRs).[33] This microstructural model is visually similar to some theoretical structural models, such as Stillinger's model,[39] modified continuous random network model by Greaves,[40] island of mobility model of Johari-Goldstein,[25,31,32] entropy and density fluctuation

model by Ediger,[41] the concept of cooperatively rearranging region and its correlation length by Donth,[42,43] and so forth.

The characteristic feature of the present model is that SBRs are surrounded by WBRs, where the atoms move relatively fast and the β relaxation takes place. In this model, the US vibrations accelerate crystallization of WBRs via β relaxation process. The model is applicable especially to metallic glasses that have a high fragility of viscosity, because the β relaxation is generally observed for fragile glasses.[39]

C. Collective vibrational motions of strongly bonded regions

We address another ultrasonic effect expected from the microstructural model in Fig. 4. On the basis of the experimental facts that (i) the US-induced crystalline phases possess a similar composition to the initial amorphous matrix[14] and (ii) the crystallization time under US vibrations becomes shorter as the US-strain amplitude is larger [Fig. 1(b)], we can suppose that crystallization is further assisted by collective vibrational motions of SBRs. This concept is similar to that proposed by Mizubayashi *et al.*[20] and Mizubayashi and Okuda[21] for explaining rapid crystallization by electropulsing. Especially, the latter experimental result (ii) is a characteristic feature of the supercooled liquid state (at 330 °C $>T_g$), because the elasticity of WBR is considered to be much softer than that of SBR above T_g. Therefore, when the strain amplitude of US vibrations becomes larger, the energy landscape in WBR is more significantly modified than that in SBR. Namely, due to the collective vibrational motions of harder SBRs, the softer elastic WBR is greatly strained (i.e., the spatial distribution of the US strain is more heterogeneous). This would further enhance frequency of occurrence of the unusual jumps via β relaxation process.

D. On the marked elasticity change after crystallization with a small mass-density change

As described in literature,[44] most metallic glasses are relatively fragile in comparison with oxide glasses such as silicate glasses. In general, fragile glasses exhibit some intriguing aspects in physical properties. One of those is about the elasticity. The elastic modulus changes drastically, by about 30%–50%, after crystallization, although the mass-density change is only about 1%–2% or less.[11,12,45–49] We consider the reason why the elastic modulus changes drastically upon crystallization with a very small change in the mass density. Here, by using the effective-mean-field (EMF) theory,[50] we calculate macroscopic elastic constants for the model of Fig. 4(b) and consider how they change with fractions of WBR and SBR.

In the EMF theory, the macroscopic elastic constants are given by the following recurrence formula:[50]

$$\bar{\mathbf{C}}_{(n+1)} = \left(\frac{1-(n+1)\Delta f}{1-n\Delta f}\bar{\mathbf{C}}_{(n)} + \frac{\Delta f}{1-n\Delta f}\mathbf{C}_\mathrm{I}\mathbf{A}_{(n)}\right) \times \left(\frac{1-(n+1)\Delta f}{1-n\Delta f}\mathbf{I} + \frac{\Delta f}{1-n\Delta f}\mathbf{A}_{(n)}\right)^{-1}, \quad (5)$$

where $\mathbf{C}_I$ denote the elastic constants of inclusions, $\mathbf{A}$ is the strain concentration factor expressed as

$$\mathbf{A}_{(n)} = [\mathbf{S}\bar{\mathbf{C}}_{(n)}^{-1}(\mathbf{C}_\mathrm{I} - \bar{\mathbf{C}}_{(n)}) + \mathbf{I}]^{-1}, \quad (6)$$

$\Delta f = 1/N$ (N is an arbitrary integer), $n = 0, 1, 2, \ldots, N$, $\mathbf{S}$ is the Eshelby tensor[51] calculated using $\bar{\mathbf{C}}_{(n)}$, and $\mathbf{I}$ is the unit matrix. Note that the elastic constants $\bar{\mathbf{C}}_{(0)}$ mean those of the initial matrix; in the present case, they are either those of SBR or of WBR. The macroscopic elastic constants $\bar{\mathbf{C}}_{(n+1)}$ of a composite with an inclusion fraction $f=(n+1)\Delta f$ can be obtained by the successive calculations. In the present calculations, Δf was set at 0.001 (i.e., $N=1000$).

For the sake of simplicity, both WBRs and SBRs are assumed to be elastically isotropic. We consider a case corresponding to metallic glasses; Poisson's ratios in SBRs are fairly large and close to those in WBRs. In contrast, the elastic constants of WBR are considered to be soft and to have a large Poisson's ratio; four sets of elastic constants are arbitrarily assigned for WBR (see, for details, the caption). The macroscopic elastic constants of the above mixtures are calculated using the EMF theory under the condition of spherical inclusions. As far as the magnitude relation of the elastic constants used in the calculations is retained, even when the shape of the inclusions is changed, the qualitative argument is unchanged.

Figures 5(a)–5(d) show the macroscopic elastic constants $\bar{c}_{ij}$ in the case where SBRs are embedded in the WBR matrix (i.e., the model in Fig. 4) by solid curves and those in the opposite case (i.e., the microstructural topology is reversed). We find that, when a very small amount of WBR exists in the former case, $\bar{c}_{ij}$ markedly decreases in all cases. However, when a small number of WBRs are embedded in the SBR matrix, only almost linear variation is seen. Therefore, the structure in which SBRs are embedded in WBR is appropriate for expressing the drastic change in the elastic constants upon crystallization. Then, a large mass-density change in WBR is acceptable, because the amount of WBR is quite small and therefore the overall density of the glass substance will appear to be substantially unchanged.

IV. MICROSTRUCTURAL INSIGHT FOR GLASS-TO-CRYSTAL TRANSITION OF LESS-STABLE METALLIC GLASSES

The temperature dependence of the viscosity generally follows the Vogel-Fulcher-Tammann equation,[24]

$$\eta(T) = \eta_0 \exp\left(\frac{A}{T-T_0}\right), \quad (7)$$

where η_0, $A>0$, and the Kauzmann isentropic temperature T_K is generally close to the Vogel temperature T_0, i.e., $T_0 \sim T_K$. The equilibrium viscosity diverges to infinity; in other words, the diffusivity approaches 0, with decreasing tem-

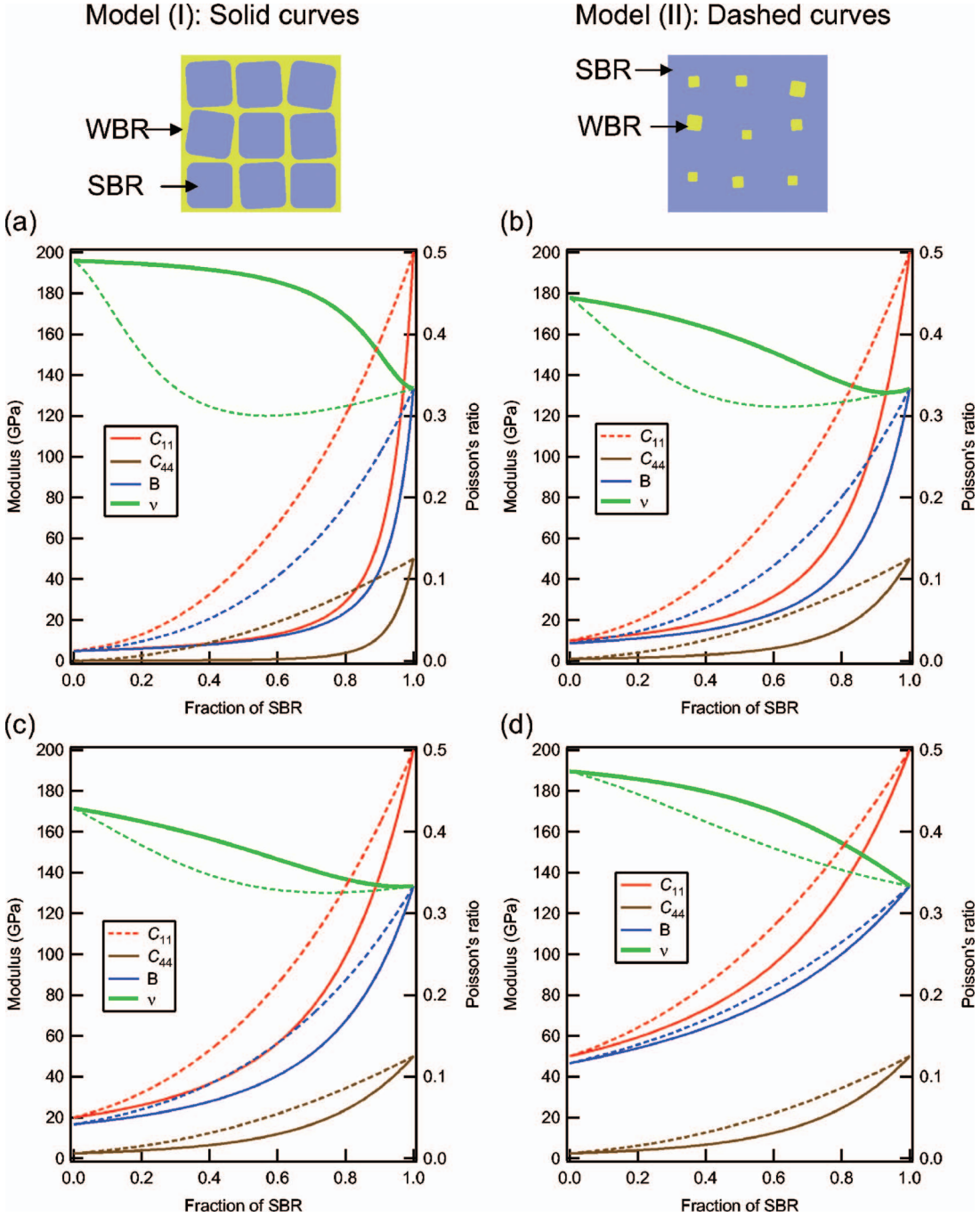

FIG. 5. (Color) Macroscopic elastic constants of glasses composed of SBRs and WBRs. The solid curves are obtained for the model (I) and the dashed curves are for the model (II). The elastic constants of SBR are set at c_{11}=200 GPa and c_{12}=100 GPa. For WBR, four sets of elastic constants are arbitrarily assigned: (a) c_{11}=5 GPa, c_{12}=4.8 GPa, (b) c_{11}=10 GPa, c_{12}=8 GPa, (c) c_{11}=20 GPa, c_{12}=15 GPa, and (d) c_{11}=50 GPa, c_{12}=45 GPa. The elastic isotropy relation $c_{44}=(c_{11}-c_{12})/2$ holds.

perature down to near $T_0(\sim T_K)$. Therefore, all the kinetic processes are ideally frozen at $T_0(\sim T_K)$. Thus, commonly observed glass transition necessarily occurs at a certain temperature above T_0 (or T_K), but it is generally recognized that the glass/liquid transition is a kinetic freezing/unfreezing phenomenon because of absence of any thermodynamic phase transformation.[52,53]

As stated earlier, stable metallic glasses usually exhibit a reversible glass↔liquid transition, whereas less-stable metallic glasses undergo the crystallization without showing the transition at conventional heating rates. However, as seen in Fig. 6, the glass transition is observable on heating at very high heating rates,[8–10] in which the values of T_g and T_x for three metallic glasses, $Pd_{42.5}Ni_{7.5}Cu_{30}P_{20}$, $Zr_{70}Cu_{30}$, and $Zr_{70}Ni_{30}$, are plotted against log β, where β denotes the heating rate. The characteristic temperatures, T_g and T_x, can be expressed in Lasocka's empirical form,[54]

$$T_{x,g} = a_{x,g} + b_{x,g} \log \beta. \tag{8}$$

It is clearly found that in all the glassy alloys, T_x is significantly raised by increasing β, because crystallization is generally a kinetic process controlled by atomic diffusion, and,

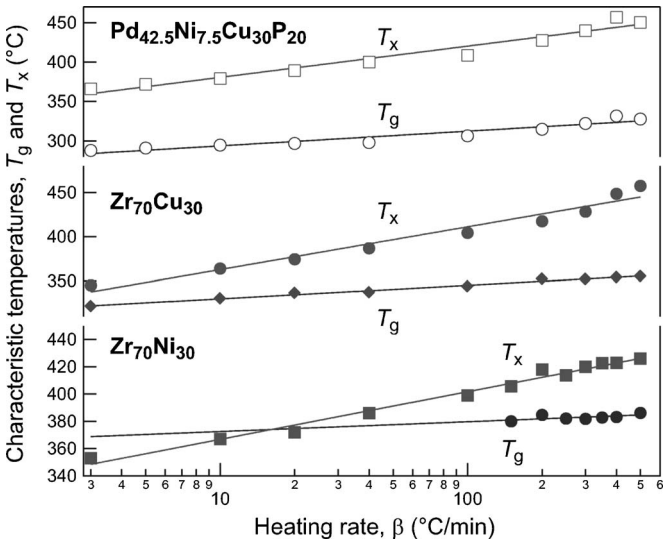

FIG. 6. Dependence of the onset temperatures of the glass transition and crystallization, T_g and T_x, on the heating rate β for three metallic glasses. These DSC data are taken from Refs. 8–10.

in contrast, the variations of T_g with β are much smaller due to collective motions of many atoms, that is, $b_x > b_g$. Therefore, there exists inevitably a temperature region of $T_x < T_g$ when $\beta < \beta_c$, where β_c is the β value at the intersection of the two curves. However, this temperature relation is quite eccentric in the light of the fact that the glass transition is a kinetic freezing phenomenon, because this indicates that motions of the constituent atoms are appreciably active below the kinetic freezing temperature T_g.

As is well known, only the β relaxation process remains active below T_g. Hence, it is reasonable to consider that the crystallization of amorphous alloys (without showing the glass-to-liquid transition) is closely associated with the β relaxation. If such active β relaxation that comes to cause devitrification took place *all over the substance*, it would be difficult to consider that the liquid-to-glass transition is caused by kinetic freezing. It is, however, a general viewpoint to consider that most of the kinetic processes are frozen in a glass substance. How do we understand this eccentric feature observed for metallic glasses? Here we propose that this feature can be understood with the microstructural model in Fig. 4. Namely, a glassy solid is spatially inhomogeneous, there are regions where atoms are easily mobile in the glassy structure, and such regions are related to the β relaxation occurring below the kinetic freezing temperature T_g. Our viewpoint based on the present experimental results is as follows. When WBRs become a liquidlike state, the glass transition occurs prior to crystallization, but when the thermal stability of WBRs is relatively low (i.e., crystallized immediately), the amorphous solid does not undergo the glass transition. Namely, the appearance of the glass-to-liquid transition depends on the degree of the thermal stability of WBR. On the other hand, thermal stability of the supercooled liquid is considered to depend on SBRs, and the role of SBRs is to inhibit occurrence of extensive atomic diffusion in WBRs at a precursor stage of crystallization. Amorphous structure in WBR would be retained till relatively high temperatures, when long-range diffusion is required for crystallization or when local atomic configurations in the amorphous phase are very different from that in the crystalline structure resulting from devitrification.[9]

Similar argument may be applicable to other types of familiar glass materials. However, they are comprised of strongly (or covalently) bonded molecules or cluster networks, so that crystallization will hardly take place below T_g. In contrast, in metallic glasses, constituent atoms do not form molecules like those in oxide and polymer glasses because of lack of covalentlike bondings, and rearrangement of atoms is relatively easy. Hence, if atomic diffusion is appreciably active even below T_g, crystallization comes to be caused. This exceptional feature of metallic glasses would be attributed to single-atom diffusion occurring at the WBRs in an inhomogeneous glassy structure.

Finally, we shall address a few remarks on the present concept for explaining the T_g and T_x behaviors of rapidly quenched (RQ) glassy alloys. In the case of RQ glassy alloys, highly excess free volume is usually quenched in the glassy state because of its high fictive temperature, which may lead to relatively high atomic mobility even in the glassy solid state. In the case of stable metallic glasses (e.g., in $Pd_{42.5}Ni_{7.5}Cu_{30}P_{20}$ and $Zr_{55}Al_{10}Ni_5Cu_{30}$), however, the relation of $T_g < T_x$ is substantially unchanged even if they are fabricated by rapid quenching and their fictive temperature is higher than the observed T_g upon heating. Hence, our present argument may be applicable, to some degree, for explanation of the observation about T_g and T_x of less-stable metallic glasses.

V. CONCLUSIONS

Structural stability of metallic glasses is likely to be deteriorated under ultrasonic perturbation at relatively low temperatures near the glass transition. As the ultrasonic-strain amplitude becomes larger, the time needed for crystallization becomes shorter.

From the mechanical spectroscopy analysis, the typical frequency for the β relaxation of $\Delta E_\beta \sim 1$ eV is found to become within a radio-frequency (megahertz) range. Hence, it is considered that the radio-frequency internal-friction behavior observed around T_g and the US-induced instability are due to the β relaxation.

In a Pd-based BMG at the very early stage of crystallization under the US annealing, the characteristic microstructure, in which crystallized wall surrounds amorphous phase, is observed. This partially crystallized microstructure allows us to infer a possible microstructural model of fragile metallic glasses that is comprised of strongly bonded regions and weakly bonded regions.

Crystallization of less-stable metallic glasses occurring below T_g (i.e., without showing the glass transition) is considered to be due to β relaxation. In the light of the general viewpoint that the glass transition is a kinetic freezing/unfreezing phenomenon, it is reasonable to consider that such an active β relaxation contributing to devitrification takes place at limited regions in a glassy structure.

ACKNOWLEDGMENTS

This work was supported by Grant-in-Aid for Scientific Research on the Priority Area Investigation of "Materials Science of Bulk Metallic Glasses" from the Ministry of Education, Science, Sports and Culture, Japan. One of the authors (T.I.) is very grateful to Kazuhiro Anazawa for his experimental support.

[1] W. Klement, R. H. Willens, and P. Duwez, Nature (London) **187**, 869 (1960).
[2] H. S. Chen and D. Turnbull, J. Chem. Phys. **48**, 2560 (1968).
[3] H. S. Chen and D. Turnbull, Acta Metall. **17**, 1021 (1969).
[4] H. S. Chen and D. Turnbull, Acta Metall. **22**, 1505 (1974).
[5] M. Telford, Mater. Today **7**, 36 (2004).
[6] S. R. Elliott, *Physics of Amorphous Materials* (Longmans, London, 1984).
[7] A. Inoue, Acta Mater. **48**, 279 (2000).
[8] T. Ichitsubo, E. Matsubara, H. Numakura, K. Tanaka, N. Nishiyama, and R. Tarumi, Phys. Rev. B **72**, 052201 (2005).
[9] T. Ichitsubo, E. Matsubara, J. Saida, and H. S. Chen, Mater. Trans. **46**, 2282 (2005).
[10] T. Ichitsubo, E. Matsubara, and H. Numakura, Mater. Sci. Eng., A (in press).
[11] T. Ichitsubo, S. Kai, H. Ogi, M. Hirao, and K. Tanaka, Scr. Mater. **49**, 267 (2003).
[12] T. Ichitsubo, E. Matsubara, S. Kai, and M. Hirao, Acta Mater. **52**, 423 (2004).
[13] T. Ichitsubo, E. Matsubara, K. Anazawa, N. Nishiyama, S. Kai, and M. Hirao, Mater. Trans. **45**, 1189 (2005).
[14] T. Ichitsubo, E. Matsubara, K. Anazawa, N. Nishiyama, M. Naito, and Y. Hirotsu, Mater. Sci. Eng., A (in press).
[15] M. Kopcewicz, U. Gonser, and H. G. Wagner, Appl. Phys. **23**, 1 (1980).
[16] M. Kopcewicz, U. Gonser, and H. G. Wagner, Nucl. Instrum. Methods Phys. Res. **199**, 163 (1982).
[17] M. Kopcewicz, H. G. Wagner, and U. Gonser, J. Magn. Magn. Mater. **40**, 139 (1983).
[18] A. Gupta, S. Lal, and R. P. Verma, J. Magn. Magn. Mater. **44**, 329 (1984).
[19] V. Keryvin, M. L. Vaillant, T. Rouxel, M. Huger, T. Gloriant, and Y. Kawamura, Intermetallics **10**, 1289 (2002).
[20] H. Mizubayashi, N. Kameyama, T. Hao, and H. Tanimoto, Phys. Rev. B **64**, 054201 (2001).
[21] H. Mizubayashi and S. Okuda, Phys. Rev. B **40**, 8057 (1989).
[22] G. Teng, Y. Chao, L. Dong, Y. Geng, and Z. Lai, Jpn. J. Appl. Phys., Part 1 **35**, 5320 (1996).
[23] Z. H. Lai, H. Conrad, G. Q. Teng, and Y. S. Chao, Mater. Sci. Eng., A **287**, 238 (2000).
[24] C. A. Angel, K. L. Ngai, G. B. McKenna, and S. W. Martin, J. Appl. Phys. **88**, 3113 (2000).
[25] G. P. Johari and M. Goldstein, J. Chem. Phys. **53**, 2372 (1970).
[26] P. G. Debenedetti and F. H. Stillinger, Nature (London) **410**, 259 (2001).
[27] H. S. Chen and N. Morito, J. Non-Cryst. Solids **72**, 287 (1985).
[28] H. Okumura, H. S. Chen, A. Inoue, and T. Masumoto, Jpn. J. Appl. Phys., Part 1 **30**, 2553 (1991).
[29] H. Okumura, H. S. Chen, A. Inoue, and T. Masumoto, J. Non-Cryst. Solids **130**, 304 (1991).
[30] J. M. Pelletier, B. Van de Moortèle, and I. R. Lu, Mater. Sci. Eng., A **336**, 190 (2002).
[31] G. Power, J. K. Vij, and G. P. Johari, J. Chem. Phys. **124**, 074509 (2006).
[32] G. Power, J. K. Vij, and G. P. Johari, J. Chem. Phys. **124**, 044513 (2006).
[33] T. Ichitsubo, E. Matsubara, T. Yamamoto, H. S. Chen, N. Nishiyama, J. Saida, and K. Anazawa, Phys. Rev. Lett. **95**, 245501 (2005).
[34] O. Yoshinari, Y. Iwata, M. Yamada, and K. Tanaka, J. Phys. III **6**, C8-613 (1996).
[35] Bo Zhang, F. Q. Zu, K. Zhen, J. P. Shui, and P. Wen, J. Phys.: Condens. Matter **14**, 7461 (2002).
[36] H. Nakajima, K. Nonaka, T. Kojima, T. Zhang, and A. Inoue, Mater. Sci. Forum **304–306**, 367 (1999).
[37] H. Nakajima, T. Kojima, T. Zumkley, N. Nishiyama, and A. Inoue, in *Proceedings of International Conference on Solid-Solid Phase Transformations '99*, edited by M. Koiwa, K. Otsuka, and T. Miyazaki (The Japan Institute of Metals, Sendai, 1999), p. 441.
[38] M. Wollgarten, S. Mechler, E. Davidov, N. Wanderka, and M.-P. Macht, Intermetallics **12**, 1251 (2004).
[39] F. H. Stillinger, J. Chem. Phys. **89**, 6461 (1988).
[40] G. N. Greaves, J. Non-Cryst. Solids **71**, 203 (1985).
[41] M. D. Ediger, J. Non-Cryst. Solids **235–237**, 10 (1998).
[42] E. Donth, J. Non-Cryst. Solids **53**, 325 (1982).
[43] E. Hempel, G. Hempel, A. Hensel, C. Schick, and E. Donth, J. Phys. Chem. B **104**, 2460 (2000).
[44] J. Basu and S. Ranganathan, Sadhana: Proc., Indian Acad. Sci. **28**, 783 (2003).
[45] D. Weaire, M. F. Ashby, J. Logan, and M. J. Weins, Acta Metall. **19**, 779 (1971).
[46] L. M. Wang, W. H. Wang, R. J. Wang, Z. J. Zhan, D. Y. Dai, L. L. Sun, and W. K. Wang, Appl. Phys. Lett. **77**, 1147 (2000).
[47] Bo Zhang, R. J. Wang, D. Q. Zhao, M. X. Pan, and W. H. Wang, Phys. Rev. B **70**, 224208 (2004).
[48] H. S. Chen, J. Appl. Phys. **49**, 3289 (1978).
[49] H. S. Chen, J. T. Krause, and E. Coleman, J. Non-Cryst. Solids **18**, 157 (1975).
[50] M. Tane and T. Ichitsubo, Appl. Phys. Lett. **85**, 197 (2004).
[51] T. Mura, *Micromechanics of Defects in Solids*, 2nd ed. (Martinus Nijhoff, The Hague, 1987).
[52] M. D. Rintoul and S. Torquato, Phys. Rev. Lett. **77**, 4198 (1996).
[53] L. Santen and W. Krauth, Nature (London) **405**, 550 (2000).
[54] M. Lasocka, Mater. Sci. Eng. **23**, 173 (1976).